ADVANCED NANOBIOMED RESEARCH Open Access
www.advnanobiomedres.com

Impact of Interfacial Viscosity on the Robustness of Phospholipid-Decorated Fluid Cell Scaffolds

*Junhong Zhou and Jun Nakanishi**

The mechanical properties of the cellular microenvironment contribute significantly to cell behavior. Thus, deformable phospholipid-decorated perfluorocarbon interfaces have emerged for further expansion of material mechanics to an ultimate soft range as cell scaffolds. In addition, a highly deformable state requires the material to be robust enough to adapt to dynamic cellular forces. However, the effect of interfacial viscosity on the cell adhesion behavior and material robustness remains unknown on the super-soft substrate. To address these issues, an interfacial phospholipid membrane (IPLM) with tunable viscosity is constructed by varying the mixing ratio of saturated and unsaturated lipid layers. By co-assembling a cell adhesive and fluorescent lipid into the IPLM, it is shown that higher viscosity interfaces with lower unsaturated lipid content are preferred from the viewpoint of cell spreading. However, a viscosity that is too high for 0% unsaturated lipid alters the lipid layer to a brittle solid-like nature, making it less adaptive to cell traction-induced high deformation. Therefore, at least a trace amount of unsaturated lipids is required to maintain the robustness of fluid scaffolds. These findings are useful for the design of biomimetic materials and the long-term investigation of cell-matrix mechanical interactions in highly adaptive environments.

1. Introduction

Cells in biological tissues reside within the extracellular matrix (ECM). The ECM, consisting of water, proteins, and polysaccharides, not only provides structural support to cells but also regulates cell behavior through biochemical and biophysical cues, influencing normal development and pathological processes. Recently, it has been widely recognized that the biophysical properties of ECM, particularly its mechanical properties, strongly affect cell behavior.[1] Mesenchymal stem cells adapt to the elasticity of the model ECM and change their morphology on variable-compliant polyacrylamide gels by rearranging their cytoskeletons to differentiate into specific lineages.[2] However, native ECM not only exhibits elastic properties but also has a viscous nature with time-dependent mechanical properties.[3]

It has been found that the loss modulus (G'') measured at 1 Hz is ≈10% of the storage modulus (G') in soft tissues (brain) and stiffer skeletal tissues (bone).[3a] Recently, hydrogels with tunable viscoelastic properties have been developed by changing their molecular weight and through covalent or ionic crosslinking, revealing that viscosity also plays a significant role in influencing cell behavior, such as cell spreading.[3] Further to this bulk mechanic tuning, a simple model system for manipulating viscosity has been developed using supported lipid bilayers (SLBs). SLBs, which exhibit a long range of lipid lateral mobility within lipid membranes assembled on a solid-supported surface, have revealed the effect of the interfacial viscosity on cell behavior.[4–8] For example, Bennett et al. used SLB systems composed of either saturated or unsaturated phospholipids with melting temperatures higher or lower than ambient temperature to investigate cell behavior at the SLBs with two distinct states of viscosities. The viscosity of these SLBs drives the mobility of the ligands present on the surface, resulting in an enhanced cell-spreading area and mechanosensitivity with increasing viscosity.[8] Furthermore, by changing the underlying substrate from a rigid solid support to a soft polymer support, SLBs can mimic the physiological flexibility of the cellular environment.[4] However, these SLBs, together with hydrogels, are limited in their ability to reach the super-soft region of mechanics, which is needed to further expand the viscoelastic window of model ECMs.

A fluid interface consisting of two liquid phases has been employed to expand the ultimate soft range of cell scaffolds in

J. Zhou, J. Nakanishi
Research Center for Macromolecules and Biomaterials
National Institute for Materials Science (NIMS)
1-1 Namiki, Tsukuba, Ibaraki 305-0044, Japan
E-mail: NAKANISHI.Jun@nims.go.jp

J. Zhou, J. Nakanishi
Graduate School of Advanced Science and Engineering
Waseda University
3-4-1 Okubo, Shinjuku-ku, Tokyo 169-8555, Japan

J. Nakanishi
Graduate School of Advanced Engineering
Tokyo University of Science
6-3-1 Niijuku, Katsushika-ku, Tokyo 125-8585, Japan

J. Nakanishi
Research Center for Autonomous Systems Materialogy (ASMat)
Institute of Integrated Research (IIR), Institute of Science Tokyo (Science Tokyo)
4259 Nagatsuta-cho, Midori-ku, Yokohama, Kanagawa 226-8501, Japan

The ORCID identification number(s) for the author(s) of this article can be found under https://doi.org/10.1002/anbr.202500076.

DOI: 10.1002/anbr.202500076

mechanobiology, as the fluid interface is intrinsic to a super-soft nature derived from its original liquid phase. For example, our group succeeded in using an interfacial phospholipid membrane (IPLM), which utilizes planar phospholipid membranes assembled at the water-perfluorocarbon (PFCL) interface. This IPLM has identified a unique cell adhesion behavior, termed cellular adaptive wetting. This adaptive wetting involves a high out-of-plane deformation of the IPLM in response to cellular forces, enabling the readout of the cellular mechanical energy output with negligible energy dissipation by taking advantage of the super-soft nature of the fluid interface.[9] Nevertheless, how the interfacial viscosity of IPLM affects cell adhesion remains poorly understood. In addition, high-strain conditions can either make materials prone to cracks that propagate to a large scale within materials or exhibit resistance to cracks (robustness) in materials science in general. The high out-of-plane deformation capability of the IPLM may also exhibit such characteristics under different viscosities. Such a correlation between IPLM robustness and interfacial viscosity needs to be explored to optimize the material properties of cell scaffolds.

To address these two aspects, this study utilized a facile method simply altering the mixing ratio of saturated and unsaturated lipids for the systematic manipulation of IPLM viscosity to investigate the influence of systematically tunable interfacial viscosity on cell adhesion behavior and materials robustness. Here, we defined viscosity as the range of the mobility of lipid molecules within the IPLM, in a similar fashion to the viscosity of reported SLBs.[8] Specifically, we used lipids with unsaturated (1,2-dioleoyl-*sn*-glycero-3-phosphocholine, DOPC) and saturated (1,2-distearoyl-*sn*-glycero-3-phosphocholine, DSPC) tails as primary components (**Figure 1**a). In this system, saturated DSPC exhibits a gel-like and poorly mobile state,[10,11] while mixing with unsaturated lipids like DOPC disrupts the intermolecular packing between saturated lipid tails, increasing lipid mobility and significantly affecting overall membrane viscosity. Typical lateral mobility was expected to be manipulated by altering the mixing content of the unsaturated lipids (Figure 1b).[5,12] For the assembly process, the lipids were prepared as mixed lipid vesicles, and the lipid membrane was formed spontaneously by incubating the vesicles and fluid interface under the proposed vesicle fusion at the water-PFCL interfaces (Figure 1c).[13] By introducing arginine-glycine-aspartic acid (RGD)-conjugated 1,2-distearoyl-*sn*-glycero-3-phosphoethanolamine (DSPE) and fluorophore-conjugated 1,2-dipalmitoyl-*sn*-glycero-3-phosphatidylethanolamine (DPPE), the IPLM allowed cell adhesion and visualization by fluorescence microscopy. In this study, Madin-Darby canine kidney (MDCK) cells stably expressing lifeact-green fluorescent protein (GFP) were chosen because these cells undergo mesenchymal-like phenotypic changes upon manipulation of environmental factors, and fluorescent labeling of the actin

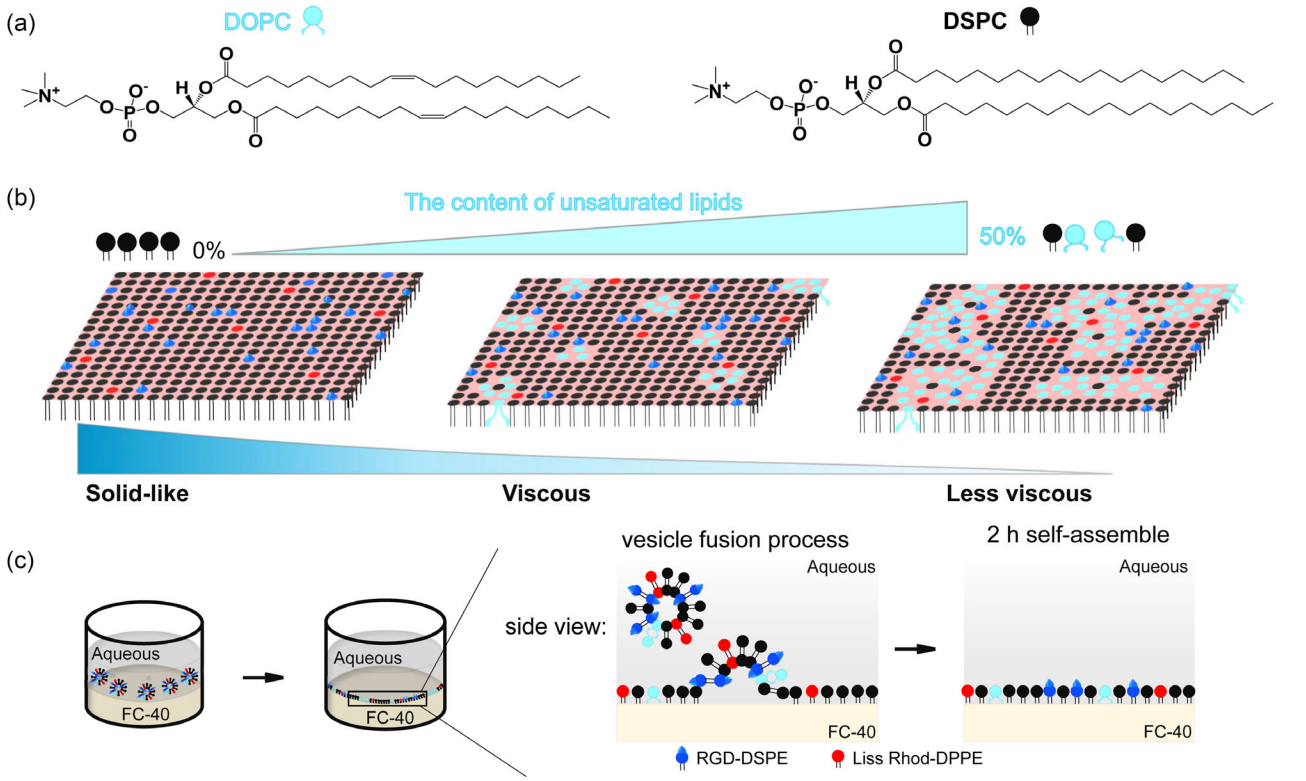

Figure 1. Viscous tuning of phospholipid membranes at the fluid interface depending on the mixing ratio of saturated and unsaturated lipids. a) Chemical structure of two primary lipids, namely DOPC and DSPC. DOPC and DSPC are shown in cyan and black, respectively. b) Schematic drawing illustrating the variation of IPLM viscosity as a function of unsaturated lipid content. The bar increments represent the content of DOPC changes. The bar decrements represent the viscous changes of IPLM. c) Scheme of the proposed formation process of IPLM at the water–PFCL interface via vesicle fusion. The lipid membranes also contain cell-adhesive RGD-DSPE (blue headgroup with saturated C-18 tail) and fluorescent Liss Rhod-DPPE (red headgroup with saturated C-16 tail).

cytoskeleton facilitates morphological observation.[14,15] After seeding the MDCK cells onto the IPLM systems, we hypothesized that cell spreading morphology and materials robustness in response to cellular forces would change depending on the viscosity of the IPLM.

2. Results

2.1. Impact of Unsaturated Lipid Contents on the Phase Behavior in IPLM

To manipulate the viscosity of the substrate, we changed the mixing ratio of the saturated and unsaturated lipids, which allowed us to construct IPLM with different mobilities. Figure S1, Supporting Information, shows a scheme of IPLM coating at a planar interface. Briefly, a continuous phospholipid membrane was expected to form at the water-PFCL interface via adsorption, fusion, rupture, and merging.[13,16] In this IPLM, RGD-DSPE, and Liss Rhod-DPPE with saturated acyl chains were introduced as cell adhesion ligands and fluorescent probes, respectively, for the membranes (Figure S1a, Supporting Information). The percentages of these two lipids in the total lipid content were fixed at 2% and 0.5%. Subsequently, varying the molar fractions (up to 50%) of DOPC and saturated lipids (DSPC + 2% RGD-DSPE + 0.5% Liss Rhod-DPPE) were used to change the mobility of the IPLM, in which DOPC and DSPC acted as primary components.

First, we studied the phase behavior at the liquid–liquid interface using fluorescence microscopy. **Figure 2**a shows representative images of the distribution of Liss Rhod-DPPE fluorophores in the six mixed lipid samples (0%, 2.5%, 5%, 10%, 20%, and 50%) investigated at ambient temperature. At 0% DOPC, the images showed apparent homogeneity based on the fluorescence images, as all lipids with saturated acyl chains were tightly packed.[17] As the DOPC content increased to 2.5%, 5%, and 10%, the fluorescence was evenly distributed over the entire surface, similar to that of the pure saturated lipid surface (0% case). Within this range (0%–10%), it was likely that the small amounts of unsaturated DOPC molecules were trapped as nanoscale domains within the DSPC-rich homogeneous background without affecting the overall fluorescence appearance, owing to the diffraction limit of optical imaging.[18] At 20% DOPC, the interface was divided into two regions: island-like fluorescent microdomains surrounded by a dark background (Figure S2, Supporting Information). Nanoscale phase separation may also occur in both fluorescent and dark domains.[18] At 50% DOPC, domain separation became more apparent, with fluorescent domain sizes reaching hundreds of microns, suggesting macroscopic phase separation of the primary components (DSPC and DOPC). In addition, another IPLM system incorporating unsaturated Liss Rhod-DOPE fluorophore and RGD-DOPE ligand—replacing Liss Rhod-DPPE and RGD-DSPE—was fabricated to determine which lipid dominated the fluorescent regions. Similar to Figure 2, homogeneity was observed for 0%–10% samples and macroscopic phase separation for 20%–50% samples (Figure S3, Supporting Information).

To confirm that the homogeneous phases observed in 0%–10% samples were not unstable, nonequilibrium states, we incubated the interface for 15 h. Homogeneous distributions were maintained within the 0%–10% DOPC range (Figure 2b), indicating no optically detectable phase separation occurred even over long timescales, proving stable lipid distribution during the experiments. The segregation of fluorescent and dark domains was also retained in the 20% and 50% IPLM samples, with randomly distributed fluorescent domains persisting in the dark background after 15 h of incubation. In addition, the contrast between bright and dark regions was slightly reduced owing to increased fluorescence in the dark regions, likely from minor migration of saturated Liss Rhod-DPPE fluorophore from fluorescent to dark domains (Figure 2b, 20% and 50%). This phenomenon did not appear with the unsaturated Liss Rhod-DOPE fluorophore (Figure S3, Supporting Information). The phase separation-mediated domain formation at sizes comparable to cells led us to propose that excessively large phase domains (microns to hundreds of microns) may cause local heterogeneous mobility.[19] Such domains could hinder investigation of the relationship between interfacial viscosity and cell adhesion owing to their nonuniformity. To determine whether the phase behavior was unique to fluid interfaces, we also constructed solid-supported phospholipid membranes with the same DOPC contents (0%, 2.5%, 5%, 10%, 20%, and 50%)

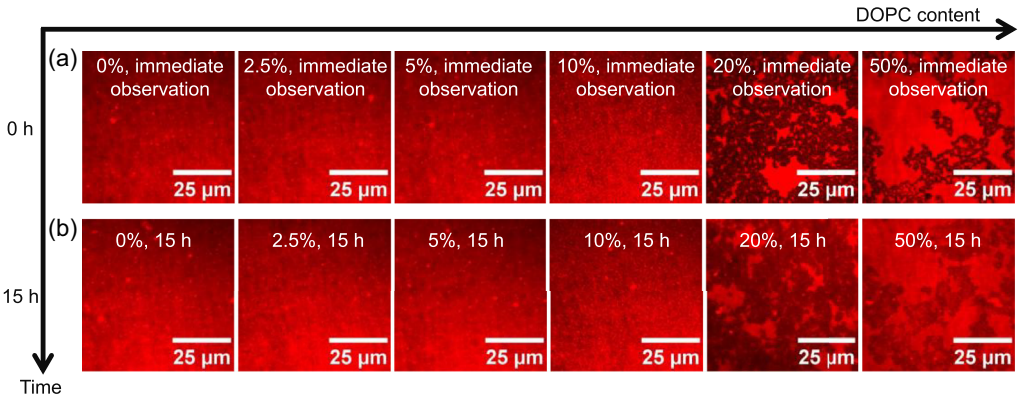

Figure 2. Fluorescence microscopy images of lipid distribution by altering DOPC content in saturated lipids from 0% to 50%. The top and bottom panels correspond to each image of a) immediately after DOPC addition and b) after 15 h. The images shown in Figure 2 are the representative fluorescence images of the lipid distribution from more than 20 independent experiments.

(Figure S4, Supporting Information). As shown in Figure S5, Supporting Information, apparently homogeneous distributions were observed in 0%–10% samples and sustained over one day, similar to the fluid interface. Notably, in 20%–50% samples, phase separation domains appeared but were smaller than those on the fluid interface, indicating that the effect of DOPC content on phase behavior was not specific to the fluid interface, although higher fluidity of the fluid interfaces accelerated domain coalescence into larger phase-separated regions. Overall, at low DOPC content, IPLMs remained in a homogeneous phase without macroscopic phase separation, while at high DOPC content, large-scale phase separation occurred, potentially complicating analyses of interfacial viscosity and cell adhesion owing to nonuniformity.

2.2. Evaluation of Interfacial Mobility Change by Altering Unsaturated Lipid Contents

To investigate the relationship between interfacial mobility and lipid composition in IPLM, we performed fluorescence recovery after photobleaching (FRAP) experiments (Figure S6, Supporting Information, and Section 5.5). This also helped indicate whether unsaturated lipids dominate the fluorescent region upon phase separation. **Figure 3**a shows fluorescence image changes during FRAP experiments for varying DOPC contents. At low DOPC content (0%–2.5%), little to no recovery was observed, and the bleached dark spots remained unchanged during the observation period. As DOPC content increased to 5%–10%, fluorescence intensity (F.I.) within the bleached spots increased, and their area decreased by 30 min. For the 20% sample, the phase-separated domains were similar in size to the bleached regions, making it difficult to selectively bleach either dark or fluorescent regions. Photobleaching the mixed domains resulted in complex recovery behavior, presumably owing to differing recovery rates between regions. In the 50% sample, a clear difference in recovery between the red fluorescent and dark regions was observed, even though the dark regions contained small fluorescent islands (Figure 3a, 50% bright and 50% dark). The bright region showed near-complete recovery at 30 min, while the dark mixed regions showed heterogeneous but detectable recovery, with bleached spots visible immediately after irradiation (Figure S7, Supporting Information, 0 min). These differing recovery rates for the bright and dark regions indicated that unsaturated lipids may be partitioned into the fluorescent domains. To further confirm whether the bright regions were dominated by unsaturated DOPC, we also investigated the system using the unsaturated Liss Rhod-DOPE fluorophore in FRAP experiments (Figure S8, Supporting Information). A similarly fast recovery was observed in the 50% sample's bright regions. Thus, regardless of the fluorophore conjugated lipid base, the bright regions were mobile phase-dominated. Considering Liss Rhod-DPPE behaved in a similar fashion to the unsaturated Liss Rhod-DOPE fluorophore, probably the bright regions were DOPC-rich regions. In addition, gradual drift of the entire membrane was observed

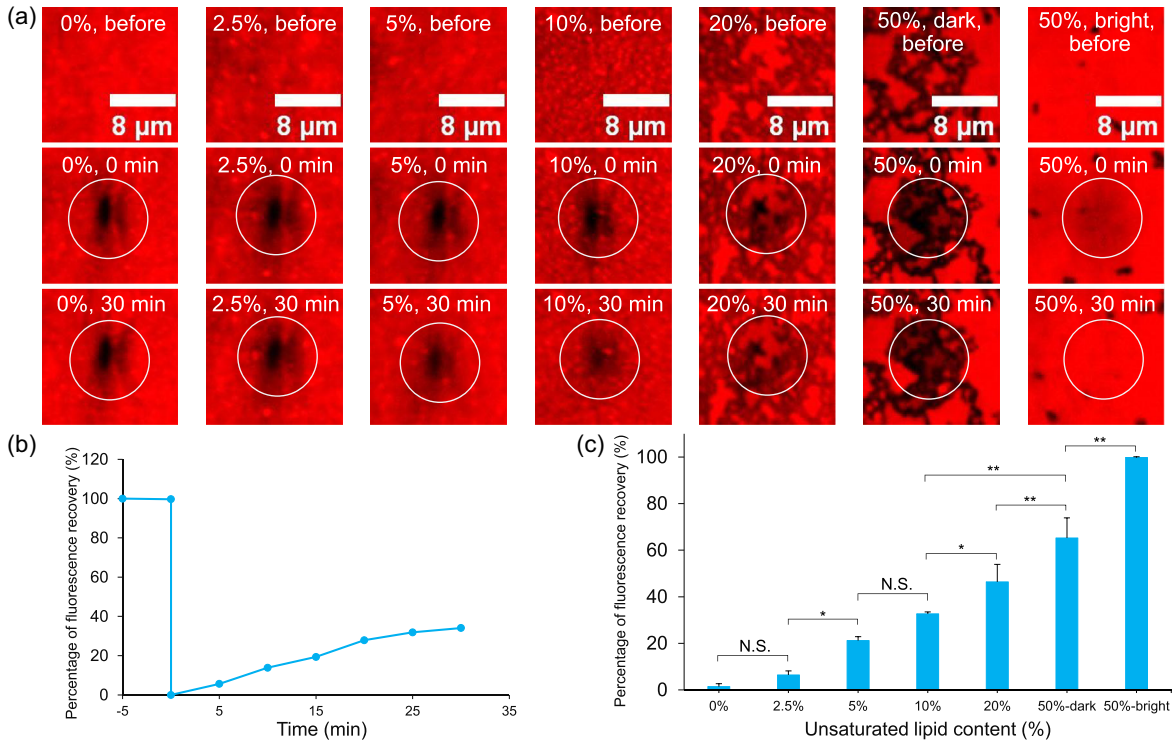

Figure 3. Evaluation of the mobility of the assembled IPLM by FRAP measurement. a) Fluorescence images of each sample taken before photobleaching, at 0 min, and at 30 min after photobleaching. White circles indicate the position of the bleached spots. b) A typical schematic plot of time-dependent fluorescence recovery profiles. c) Quantitative analysis of the percentage of fluorescence recovery in the FRAP experiment shown in (a). F.I. values in the bleached regions were normalized to the value before photobleaching. Each condition was tested three times. Statistical differences were analyzed using One-way ANOVA: $*p < 0.05$, $**p < 0.01$, $***p < 0.001$, N.S., not significant ($p \geq 0.05$).

in the 20% and 50% samples. This drift was likely owing to the increased presence of unsaturated lipids forming a continuous phase, where the highly mobile unsaturated lipids were no longer constrained by saturated lipid-rich domains.[20]

By considering the general fluorescence profile during FRAP (Figure 3b and S6), we quantified the mobility of IPLM in terms of the percentage of fluorescence recovery from the F.I. of the bleached region before and after 30 min of photobleaching (See Experimental for details). As shown in Figure 3c, we observed a gradual increase in the recovery of the apparently homogeneous membrane with a DOPC content of 0%–10%. Similar trends were observed for systems using unsaturated Liss Rhod-DOPE fluorophores (Figure S8, Supporting Information) and solid-supported lipid membranes in the 0%–10% range (Figure S9, Supporting Information). Therefore, the presence of trace amounts (up to 10%) of unsaturated lipids enabled control of the overall mobility of the IPLM samples, depending on the DOPC content. Moreover, there was no significant difference in membrane mobility between those on the solid support and the fluid interface for the 0% and 2.5% samples (Figure S10, Supporting Information), which may be attributed to the roles of intermolecular interactions of each lipid (Van der Waals force) in the overall membrane mobility rather than the mobility and/or friction of lipid molecules against the subphase. Slower mobility was observed for the 5% and 10% samples on the solid-supported surface than for the same samples on the fluid interface, suggesting that the type of sub-phase regulated the mobility of the coating in this range. Further increasing the DOPC content to 20% and 50% abolished the dependence of the mobility on the subphase, owing to the high mobility of the lipid membranes. Therefore, the subphase type affected lipid mobility within a limited range of DOPC content.

However, at 20% DOPC content, with comparable sizes of the phase separation domains and bleached spots, the heterogeneous recovery in the mixed domains resulted in a large variation in the average recovery rate. When the DOPC content was further increased to 50%, with an enlarged phase separation of the red fluorescent and dark domains, the recovery rate within the red fluorescent domains was significantly higher than that in the dark region, where the recovery rate was somewhat overestimated owing to the presence of mixed small fluorescent islands. Simultaneously, a 50% DOPC-containing sample using the unsaturated Liss Rhod -DOPE fluorophore exhibited a similar rate of recovery (Figure S11, Supporting Information), further supporting that the red fluorescent domain corresponded to the unsaturated lipid-rich phase. To quantify the viscosity change of the respective sample, the diffusion coefficient (D) and the relationship between the diffusion coefficient and the viscosity (η) based on the Saffman–Delbruck model were roughly measured from FRAP recovery profiles using unsaturated Liss Rhod-DOPE fluorophore for 10%–50% samples (Figure S11, Supporting Information).[4a,8,21] The general increase in the diffusion coefficient (Figure S12a, Supporting Information) and decrease in viscosity (Figure S12b, Supporting Information) were indicative of a much higher mobility of the IPLM by increasing the DOPC content. Overall, the DOPC-dependent increase in fluorescence recovery of the IPLMs across the 0%–50% range demonstrated that the viscous nature of IPLM was finely tuned by altering DOPC content.

2.3. The Impact of IPLM Viscosity on Cell Spreading Behavior

After establishing the viscosity-tunable platform, we cultured Lifeact-GFP MDCK cells on the IPLMs for 3 h and 6 h to observe how tunable interfacial mobility influences cell adhesion, particularly during early cell–IPLM interactions. As shown in **Figure 4**a, spreading cells were observable on the 0%–5% DOPC samples, with a general decreased tendency in spreading area among these samples at the 3 h time point (Figure 4b, inset). In contrast, for DOPC contents above 10%, almost no cell spreading was observed, indicating that cells were unable to form a

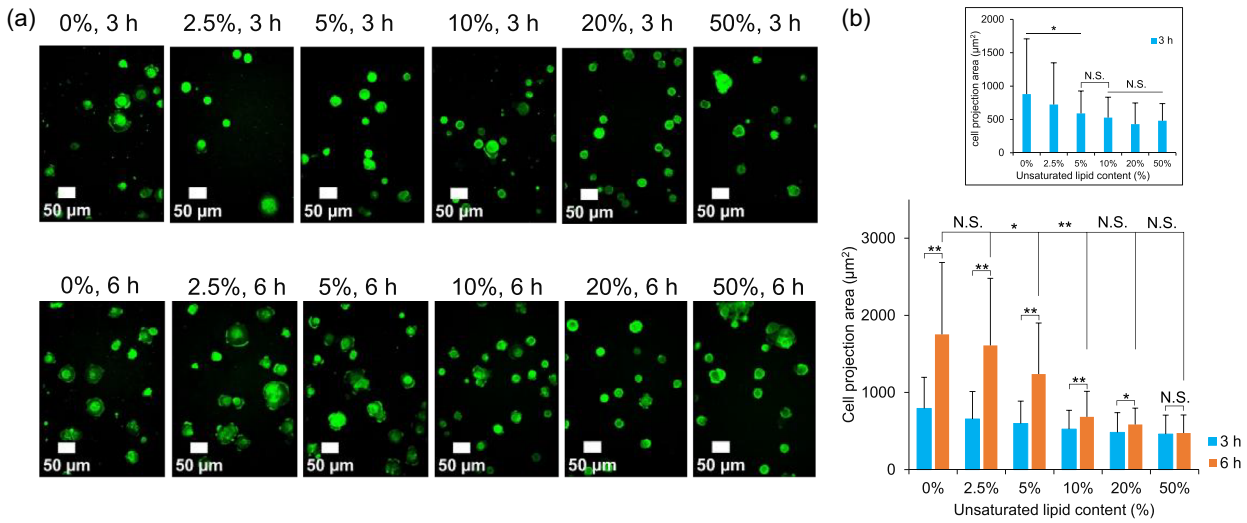

Figure 4. Representative images of cellular adhesion behavior at the IPLM with different DOPC content. a) Cell spreading morphology at the IPLMs after seeding cells for 3 h and 6 h, respectively. Green: Lifeact-GFP. b) Quantitative analysis of the relationship between cell spreading area and unsaturated DOPC content. Inset: magnified data from the 3 h condition. The number of cells was 50 for each condition. Statistical differences were analyzed using One-way ANOVA: *$p < 0.05$, **$p < 0.01$, and ***$p < 0.001$, N.S., not significant ($p \geq 0.05$).

stable bond with the ligands on these highly mobile membranes. These results suggested that less mobile IPLMs (0%–10% DOPC) were necessary to support initial cell adhesion within a 3 h timeframe.

After extending the incubation time to about 6 h (Figure 4a,b, 6 h case), the cells enhanced spreading with expanding lamellipodia, which was the appearance for early-stage cell spreading. No significant difference in the cell spreading area was observed at 0–2.5%, indicating that the effect of IPLM viscosity on the cell spreading behavior reached a saturation level in the range of 0–2.5% DOPC content. Subsequently, a slight decrease in the spreading area was observed at 2.5%–5%. Thereafter, a sharp decrease was found to be significantly affected by 5%–10% DOPC content. As the mobility increased from 10% to 20% IPLM, no significant difference was observed between these two cases, while cells started to spread compared to their 3 h condition. For the 50% sample, no further spreading was observed compared to the 3 h, 50% sample. In addition, some cells tended to form aggregates in the 50% sample (Figure 4a, 50%, 6 h). This behavior was consistent with that reported in the literature,[14] where MDCK cells either spread or coalesced to form aggregates depending on the interfacial relaxation time of the polymeric scaffolds. Pulling all 6 h data together confirmed that cell spreading was influenced by IPLM mobility. In the 2.5%–10% DOPC range, increasing mobility correlated with reduced cell spreading. Additionally, a mobility threshold appeared to be required to support significant cell spreading on less-mobile IPLMs, specifically below 10%. In contrast, cell spreading was poor, with a round morphology observed on more mobile IPLMs (above 10%). Thus, the key difference in the initial cell adhesion on the IPLMs was the rate of spreading, which was strongly modulated by interfacial mobility.

In contrast, cells on the solid surface showed an enhanced spreading morphology compared to those on the fluid counterpart (Figure S13, Supporting Information). This is not surprising considering that cell adhesion is not only regulated by interfacial viscosity but also by bulk mechanics. It should be noted that instead of limited spreading, the fluid interface allows adaptive wetting with out-of-plane deformation[9] where another criterion, mechanical robustness, plays a critical role in maintaining the integrity of the cell scaffold; this will be discussed in the next section.

2.4. Impact of Viscosity on the Robustness of IPLM

The observed similar dependence of fluorescent lipid mobility (Figure 3c) and cell spreading (Figure 4b) on DOPC content indicated successful control of the interfacial viscosity of the entire lipid membrane. In addition, we observed the condensation of the fluorescent lipids in terms of increased F.I. under the cells (**Figure 5**a, magnified area of the dashed rectangle for the 0% sample and the corresponding line scan). Furthermore, this condensation was observed regardless of whether the fluorophore was conjugated to a saturated or an unsaturated backbone (Figure S14, Supporting Information). Considering that cells applied forces to the IPLM by dragging the RGD ligands rather than the fluorescent lipid, these observations indicated that other lipid components also moved along the cellular traction forces.

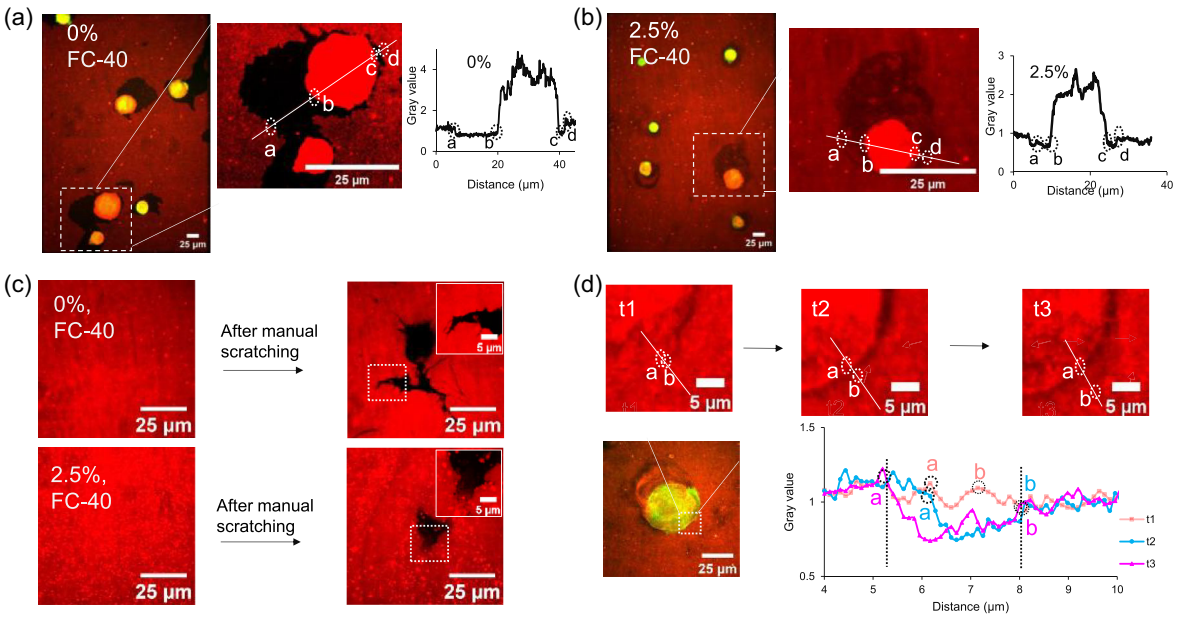

Figure 5. Evaluation of the robustness of IPLM with FC-40 subphase. a) Representative fluorescence micrograph of adherent cells inducing defect regions in the 0% sample and b) slight fluorescence depletion in the 2.5% sample at the FC-40–water interface. The area of the dashed rectangle is magnified on the right. The locations of the edge of the defect or depletion and cells are indicated as a, b, c, and d. The corresponding line scan of F.I. and the marked locations a, b, c, and d in the magnified image are shown below. Green: Lifeact-GFP. Red: Liss Rhod-labeled lipid. c) In situ fluorescence image of IPLM in its pristine (left) and manually fractured states (right). The area of the dashed rectangle is magnified in the inset (top right). d) The process of crack formation at the FC-40–water interface over time at the cell periphery. The area of the dashed rectangle is magnified in the upper image. The location of the edge of the crack is marked as a and b. The corresponding line scan of F.I. and marked locations a and b are shown at the lower right.

At the same time, a dark zone with depleted fluorescence was observed around the cells after 3 h for the 0% sample. According to the reported findings,[22] a dilatational storage modulus of phospholipid monolayer at the oil–water interface is higher than the loss modulus. Especially, lipids with phosphatidylethanolamine (PE) headgroup at high-strain state (higher than 20%) could exhibit wrinkle formation, indicating jamming (which is solid-like elastic transition) at the oil–water interface, whose behavior could be linked to the formation of highly elastic interfaces. Thus, the observed condensation of Liss Rhod-DPPE and RGD-DSPE, leading to dark zones (namely defect regions), suggested a limited range of lateral movement of the entire lipids in the timescale of experimental 3 h against cellular force dragging, that overall lipid mobility became limited under prolonged cellular force dragging, exhibiting a solid-like elastic behavior. Furthermore, trace levels of fluorescence within the defect regions (Figure 5a, line scan of the 0% sample) suggested coexistence of lipids and proteins from the culture medium, likely owing to a relatively diluted lipid layer exposed to a critical protein concentration.[23] To confirm the composition of the cell force-induced defect regions, fluorescein isothiocyanate labeled-bovine serum albumin (FITC-BSA) was introduced into the culture medium. Both medium-derived protein labeled in green and red fluorescent lipids were observed in a coexistence fashion (Figure S15, Supporting Information). In contrast, IPLM with a small amount of DOPC content (2.5% ratio) showed local accumulation but less macroscopic depletion (consumption of fluorophore) around the cells (Figure 5b, 2.5% sample). Such a reduction in lipid depletion in the dark region could be caused by enhanced lipid reorganization and/or insufficient ligand dragging due to the increased mobility of the lipid layers in the presence of 2.5% unsaturated DOPC. In addition, considering that high out-of-plane deformation was involved in the adaptive wetting behavior, as reported in our previous work,[9] tailoring the interfacial tension was required to induce a high deformation state with cellular force efficiently transferred to the IPLM. This approach could be utilized to exclude the factor of insufficient ligand dragging. When the cell force induced high out-of-plane deformation by changing the oil phase from FC-40 to FC-70 (lower interfacial tension), the dark region of the 0% sample became more significant in the top and side views (Figure S16, Supporting Information, 0% sample). The low interfacial tension rendered the interface much more deformable, and thus, the cells invaded most of their body below the initial level of the water-PFCL interface.[9] Such a high degree of deformation provided a more severe mechanical stimulus to the IPLM. Within this high-deformation state, the 0% sample exhibited an enlarged defect area toward the distal position from the cell periphery. This indicated that cellular force-induced fracture occurred in lipid membranes with a solid-like nature. The viscous 2.5% IPLM behaved similarly to that observed at the FC-40 interface, although a similar level of high out-of-plane deformation of the membranes was observed (Figure S16, Supporting Information, side view of the 2.5% sample).

To directly demonstrate the impact of interfacial viscosity on the robustness of the IPLM, the mechanical compliance of the IPLM with 0% and 2.5% DOPC content was tested by physically scratching the interface under an external force. As shown in Figure 5c, after manual scratching, distinct edges of complete defect were observed for 0% IPLM, which was typical for brittle materials with little tendency to deform before fracture.[24] The moderate mobility of the 2.5% sample made it difficult to form cracks by scratching (Figure S17, Supporting Information). Even when periodic scratching caused the appearance of cracks, diffuse fluorescent fragments remained attached to the fracture edges (Figure 5c, bottom panel). This observation suggested that the purely saturated one (0%) was brittle and easily fractured by a large force owing to the short range of lipid reorganization, whereas the one with moderate mobility (2.5%) was robust and capable of lateral reorganization against large deformations.[25,26] These material characterizations provided a reasonable expectation that cell-applied forces also caused the brittle fracture of the 0% IPLM, as shown in Figure 5d. The crack formation process in the 0% sample was detected from a line scan of the F.I. around the cell periphery. The profile showed an expansion of the sharp drop in intensity over time (line scan of the marked location between locations a and b for each time point). Overall, the robustness of IPLM was controlled by altering the viscosity of the lipid membrane. Furthermore, rather than a solid-like brittle property, the IPLM required a certain degree of mobility to be robust against cellular dynamic force exertion.

3. Discussion

In this study, we aimed to investigate how the viscosity of IPLM affected cell adhesion behavior by mixing saturated and unsaturated lipids at the water–PFCL interface. DSPC was used as the primary component to construct phospholipid membranes with varying mobility by increasing the DOPC content. This further expanded the viscoelastic window into an ultra-soft range. This contrasted with previous studies based on hydrogels and solid SLBs, where viscosity tuning relies on cholesterol content,[7] lipid saturation,[8] substrate hydrophilicity,[27] and other factors. At this fluid interface, the omniphobic nature of the PFC enabled a continuous lipid monolayer to coat the interface through van der Waals interactions between hydrophobic acyl chains.[28] This suggested that the degree of acyl chain saturation may alter membrane mobility through altering Van der Waals interactions and, consequently, overall viscosity.

Thereafter, the viscosity tunability of each IPLM sample was investigated using FRAP by measuring the percentage of fluorescence recovery in a bleached spot. IPLM exhibited high viscosity with macroscopic homogeneity at low DOPC content (0%–10%), while less viscous, phase-separated domains emerged at $\geq$20% DOPC. The apparent homogeneity of low-DOPC samples was maintained over a one-day time scale. A similar dependence of interfacial mobility and cell adhesion behavior on DOPC content was observed on phospholipid-decorated perfluorinated solid surfaces, indicating that the observed effects were not specific to fluid interfaces.

Furthermore, the apparently consistent lipid movement of the overall lipid in response to cell traction forces was observed. Cell adhesion to IPLM (0%) led to the occurrence of defect regions, whereas IPLM (2.5%) remained relatively intact at the cell periphery. This characteristic of IPLM robustness was found to be strongly influenced by IPLM viscosity (Figure S18, Supporting

Information). Specifically, when cells were cultured at FC-40, local cracks driven by cell forces were observed in the 0% sample. To assess whether the saturated IPLM (0%) showed solid-like, brittle properties, high deformation driven by cell forces at the FC-70–water interface was investigated. The continuous membrane structure was stochastically disrupted, leading to macroscale lipid defects. Manual scratching also resulted in a brittle fracture. Therefore, when cellular traction forces exceeded a critical threshold, stochastic cracks and progressive fluorescent defects appeared in the 0% sample. In contrast, the robust IPLM (2.5%) consumed some fluorophores and showed less macroscopic depletion. As this IPLM could dissipate mechanical load and maintain structural integrity through lipid reorganization (Figure S18, Supporting Information), even when the entire cell body was wrapped within the PFCL phase after switching from FC-40 to FC-70 (lower interfacial tension). However, the observed relationship between IPLM mobility and robustness property contrasted with previous findings on collagen I- or fibronectin-functionalized SLBs mixed with cholesterol, where high ECM protein translocation led to local depletion.[7] Considering the difference of the subphase between IPLM and SLBs, this opposite trend may be attributed to the presence of a hydration layer between lipid membranes and the substrate in SLBs, whereas Van der Waals interactions mediated lipid assembly on tethered or liquid PFCLs. Therefore, the contrasting observations arised from differences in the adaptive nature of lipid layers under cellular traction forces. Furthermore, cells adhering to fluid interfaces experienced varying degrees of deformation, especially at high out-of-plane deformation, necessitating IPLM robustness to withstand dynamic traction forces. These findings highlighted the importance of IPLM robustness in supporting cell adhesion behavior.

4. Conclusion

In summary, we demonstrated that the mobility-tunable IPLM based on different mixing ratios of saturated and unsaturated lipids affected the cellular adhesion behavior and robustness of cell scaffolds. In the lower DOPC content range, the viscosity of IPLM evidently affected the cell adhesion behavior. MDCK cells on IPLM with high viscosity showed good spreading, while those on IPLM with low viscosity showed limited spreading, indicating the existence of a critical threshold to determine significant cell spreading. In addition, cells adhering to IPLM, composed of pure saturated lipids with a solid-like nature, caused a lipid defect on the platform. A small amount of unsaturated lipids in the IPLM may enable lateral reorganization to dissipate the loading forces and maintain an intact structure at the macroscale. Overall, the viscous nature not only affected the cellular adhesion ability but also made the IPLM robust enough to adapt to the cellular dynamic traction force. Given the role of viscosity and crack occurrence in cell adhesion, further detailed studies on the relationship between systematic mobility tuning and cellular adhesion behavior are of great interest. In addition, our study will be useful for designing biomimetic materials with varying viscosities and for technical applications requiring cell adhesion to super-soft fluid surfaces.

5. Experimental Section

Lipid Vesicle Preparation: DSPC, DOPC, RGD-DSPE, and Liss Rhod-DPPE were purchased from Avanti Polar Lipids (Alabaster, AL). The powders were dissolved in chloroform at concentrations of 10, 10, 1, and 1 mM. Stock lipid vesicle solutions were prepared in phosphate buffered saline (PBS) at a concentration of 1 mM to the desired unsaturated DOPC: saturated (DSPC: RGD-DSPE:Liss Rhod-DPPE) molar ratios at x:[(97.5%–x):2%:0.5%] after evaporating chloroform for 3 h under vacuum conditions. For changing the saturated Liss Rhod-DPPE to unsaturated Liss Rhod-DOPE, the mixing ratio was kept the same as saturated Liss Rhod-DPPE.

Fluorination of the Bottom of the Culture Chamber: The custom-designed cell culture chamber (inner wall, 21 mm; outer wall, 25 mm) was fluorinated as described previously.[9] In brief, the chambers were first treated with 10 wt% potassium hydroxide at 60 °C for 1 h, followed by rinsing with deionized water, and dried under an air stream. The bottom glass was then fluorinated with a 0.5 vol% ethanol solution of trichloro(3,3,4,4,5,5,6,6,7,7,8,8,8-tridecafluorooctyl) silane, followed by heating at 70 °C for 30 min. Finally, the glass was rinsed 2–3 times with ethanol and water for cleaning and sterilized via autoclaving.

Construction of the IPLM: Fluorination allowed FC-40 (250 µL) to wet the lower layer of the well, followed by 2 mL phosphate buffered saline (PBS). To assemble the IPLM at the water-PFCL interface, the stock lipid vesicle solution was preheated at 70 °C for 30-min, then sonicated to clarity at Room Temperature using a probe-type ultrasonic disruptor (UD-100; Tomy, Tokyo, Japan) with 10 cycles of intermittent operation (45 s of high-power sonication separated by 30 s intervals). The unilamellar vesicles were then added to the upper PBS phase to achieve a final phospholipid concentration of 0.2 mM. The IPLM self-assembly process was performed at Room Temperature for 2 h and then slowly washed by repeatedly replacing the upper PBS phase with fresh PBS. FC-40 was used as the PFCL in all systems unless otherwise stated, in which case FC-70 was used.

Construction of the Phospholipid Membrane at the Solid-Supported Surface: Fluorination enabled phospholipids to coat the surface through hydrophobic intermolecular interactions. To achieve this, the unilamellar vesicle solution (0.2 mM in 2.5 mL PBS solution) was added directly to the chamber. The self-assembly process was performed at RT for 2 h and then slowly washed by repeatedly replacing with fresh PBS.

FRAP: FRAP measurements exposed a fluorophore-labeled sample to strong light, bleaching the fluorophore and creating a bleached region. If the fluorescent molecules are highly diffusible, the bleached region recovers via diffusion from the surroundings. However, if the mobility is low, a bleached region persists. Fluorescence images were obtained using an inverted microscope (IX-81; Olympus, Shinjuku, Japan) equipped with a disc-scan confocal unit CSU10 (Yokogawa, Tokyo, Japan), an Andor laser combiner (Oxford Instruments, Oxfordshire, UK), an MD-695 CMOS camera, and a 60× water immersion objective (LUMPlanFL N; Olympus) to observe the IPLM. Micropoint laser, ablation equipped within the above microscope, was used to photobleach a spot in the desired region with 561 nm light. Fluorescence imaging was performed after specified time intervals. For the 2.5%, 5%, 10%, 20% and 50% samples, to account for potential rapid recovery immediately after bleaching, 30% of the prebleach intensity was used as the intensity at 0 min. This specific value was determined using the 0% sample, as the bleached intensity from the instrument should be consistent across all samples. The 0% sample showed almost no recovery during the 30 min FRAP experiment, making it a standard for evaluating the bleached intensity.

To quantify the varied viscosity of the respective sample, diffusion coefficient (D) and the relationship between the diffusion coefficient and the viscosity (η_m) based on Saffman–Delbruck equation were determined from FRAP recovery profiles for 10%–50% samples.[4a,8,21] According to the Equation (1), the diffusion coefficient D can be calculated for the 10% DOPC sample as an example.

$$D = \frac{{r_n}^2}{4\tau_{1/2}} \tag{1}$$

r_n is roughly estimated radius of the bleach area (in this study $r_n = 6.06$ µm). $\tau_{1/2} = 1288$ s. Thus, $D = 0.00716$ µm^2 s^{-1}. The relationship

between the diffusion coefficient D and the viscosity η_m can use Equation (2) according to the literature.[4a,8,21]

$$D = \frac{k_B T}{4\pi\eta_m h}\left(\ln\left(\frac{\eta_m h}{\eta_w R}\right) - 0.5772\right) \quad (2)$$

k_B is the Boltzmann constant, $k_B = 1.381 \times 10^{-23}\,m^2\,kg\,s^{-2}\,K^{-1}$, $T = 310\,K$ (37 °C), $\eta_w = 0.691 \times 10^{-3}$ Pa·s (the viscosity of water), $h = 3$ nm (the thickness of a lipid), $R = 0.5$ nm (the radius of a single lipid). Then the viscosi ty η_m of each sample can be calculated after the iteration calculation by Microsoft Excel.

Cell Culture: The culture medium for MDCK cells (RCB0995, RIKEN Cell Bank) expressing Lifeact-GFP was prepared by diluting with 10× minimal essential medium (MEM, Thermo Fisher Scientific, Waltham, Massachusetts, U.S.). It was supplemented with 10% heat-inactivated fetal bovine serum (EU origin, Biowest, Naullie, France), 100 units mL^{-1} penicillin, 100 µg mL^{-1} streptomycin (Nacalai, Kyoto, Japan), 1% MEM nonessential amino acids (Nacalai), 1% sodium pyruvate (Nacalai), 1% L-glutamate (Nacalai), and 2.2 g L^{-1} sodium hydrogen carbonate (Wako). The cells were cultured in a Petri dish at 37 °C in a 5% CO_2 atmosphere. Prior to seeding the cells onto the IPLM, the upper aqueous phase (PBS) of the IPLM platform was replaced with the prepared cell culture medium. For seeding onto the IPLM platform, the MDCK cells expressing Lifeact-GFP were detached from the culture dish using trypsin-ethylenediaminetetraacetic acid (Wako), plated at a density of 2×10^4 cells cm^{-2}, and incubated at 37 °C with 5% CO_2 for the desired time before observation. Images were obtained using a confocal laser-scanning microscope equipped with a 60× water objective.

Evaluation of the Robustness: First, a fluorescence microscopy image of the IPLM was obtained. The IPLM system was then manually scratched at the fluid interface using a needle. The resulting cracks were observed in situ via fluorescence microscopy. The durability of the IPLM was characterized by the presence of fragment diffusion near the edge of the crack.

Statistical Analysis: All data were not normalized prior to collation of independent experiments. Results are presented as mean ± standard deviation. The sample size for each experiment is indicated in the corresponding figure legends. Statistical analyses were performed using one-way ANOVA followed by Tukey's post-hoc test for pairwise comparisons using an online statistical tool (One-way ANOVA with post-hoc Tukey HSD Test Calculator). P values below 0.05 were considered significant.

Supporting Information

Supporting Information is available from the Wiley Online Library or from the author.

Acknowledgements

This study was supported in part by the Japan Society for the Promotion of Science KAKENHI (grant nos. 22H00596 and 23K17481 to J.N.).

Conflict of Interest

The authors declare no conflict of interest.

Author Contributions

Jun Nakanishi: conceptualization (lead); formal analysis: supporting; funding acquisition (lead); methodology (equal); supervision (lead); validation (lead); writing—review & editing (equal). **Junhong Zhou**: conceptualization (equal); data curation (lead); formal analysis (lead); investigation (lead); methodology (equal); validation (equal); writing—original draft (lead); writing—review & editing (equal).

Data Availability Statement

The data that support the findings of this study are available from the corresponding author upon reasonable request.

Keywords

cell adhesion, extracellular matrix, fluid interface, phase separation, robustness, viscosity

Received: March 17, 2025
Revised: July 4, 2025
Published online: August 22, 2025

[1] D. E. Discher, P. Janmey, Y. Wang, *Science* **2005**, *310*, 1139.
[2] a) A. J. Engler, S. Sen, H. L. Sweeney, D. E. Discher, *Cell* **2006**, *126*, 677. H. Cao, Q. Zhou, C. Liu, Y. Zhang, M. Xie, W. Qiao, N. Dong, *Acta Biomater.* **2022**, *143*, 115. b) Y. Hou, L. Yu, W. Xie, L. C. Camacho, M. Zhang, Z. Chu, Q. Wei, R. Haag, *Nano Lett.* **2019**, *20*, 748.
[3] a) O. Chaudhuri, J. Cooper-White, P. A. Janmey, D. J. Mooney, V. B. Shenoy, *Nature* **2020**, *584*, 535. b) C. Huerta-López, A. Clemente-Manteca, D. Velázquez-Carreras, F. M. Espinosa, J. G. Sanchez, Á. Martínez-del-Pozo, M. García-García, S. Martín-Colomo, A. Rodríguez-Blanco, R. Esteban-González, F. M. Martín-Zamora, L. I. Gutierrez-Rus, R. Garcia, P. Roca-Cusachs, A. Elosegui-Artola, M. A. del Pozo, E. Herrero-Galán, P. Sáez, G. R. Plaza, J. Alegre-Cebollada, *Science Adv.* **2024**, *10*, eadf9758. c) E. Qiao, C. A. Fulmore, D. V. Schaffer, S. Kumar, *Proc. Natl. Acad. Sci.* **2024**, *121*, e2317711121. d) E. Hui, K. I. Gimeno, G. Guan, S. R. Caliari, *Biomacromolecules* **2019**, *20*, 4126. e) O. Chaudhuri, L. Gu, M. Darnell, D. Klumpers, S. A. Bencherif, J. C. Weaver, N. Huebsch, D. J. Mooney, *Nat. Commun.* **2015**, *6*, 6365.
[4] a) R. Glazier, K. Salaita, *Biochim. Biophys. Acta (BBA)* **2017**, *1859*, 1465. b) W. Hao, J. Han, Y. Chu, L. Huang, J. Sun, Y. Zhuang, X. Li, H. Ma, Y. Chen, J. Dai, *Biomaterials* **2018**, *161*, 106.
[5] G. Koçer, P. Jonkheijm, *Adv. Healthc. Mater.* **2017**, *6*, 1600862.
[6] J. van Weerd, M. Karperien, P. Jonkheijm, *Adv. Healthc. Mater.* **2015**, *4*, 2743.
[7] S. Vafaei, S. R. Tabaei, K. H. Biswas, J. T. Groves, N. J. Cho, *Adv. Healthc. Mater.* **2017**, *6*, 1700243.
[8] M. Bennett, M. Cantini, J. Reboud, M. Salmeron-Sanchez, *Proc. Natl. Acad. Sci.*, **2018**, *115*, 1192.
[9] Z. Lu, M. Tenjimbayashi, J. Zhou, J. Nakanishi, *Adv.Mater.* **2024**, 2403396.
[10] F. G. Wu, H. Y. Sun, Y. Zhou, G. Deng, Z. W. Yu, *RSC Adv.* **2015**, *5*, 726.
[11] A. Koukalová, M. Amaro, G. Aydogan, G. Gröbner, P. T. F. Williamson, I. Mikhalyov, M. Hof, R. Šachl*Sci. Rep.* **2017**, *7*, 5460.
[12] A. Żak, N. Rajtar, W. Kulig, M. Kepczynski, *Membranes* **2023**, *13*, 411.
[13] C. Kataoka-Hamai, K. Kawakami, *J. Phys. Chem. B* **2020**, *124*, 8719.
[14] A. C. Chang, K. Uto, K. Homma, J. Nakanishi, *Biomaterials* **2021**, *274*, 120861.
[15] S. A. Abdellatef, J. Nakanishi, *Biomaterials* **2018**, *169*, 72.
[16] G. J. Ma, B. K. Yoon, T. N. Sut, K. Y. Yoo, S. H. Lee, W. Y. Jeon, J. A. Jackman, K. Ariga. N. J. Cho, *View* **2022**, *3*, 20200078.
[17] D. Drabik, G. Chodaczek, S. Kraszewski, M. Langner, *Langmuir* **2020**, *36*, 3826.
[18] Y. Pandey, A. Ingold, N. Kumar, R. Zenobi, *Nanoscale* **2024**, *16*, 10578.
[19] C. Paba, V. Dorigo, B. Senigagliesi, N. Tormena, P. Parisse, K. Voitchovsky, L. Casalis, *J. Colloid Interface Sci.* **2023**, *652*, 1937.

[20] N. Kahya, D. Scherfeld, K. Bacia, B. Poolman, P. Schwille, *J. Biol. Chem.* **2003**, *278*, 28109.

[21] a) D. Dey, S. Marciano, G. Schreiber, *bioRxiv* **2020**, 2020.07.01.181750. b) D. W. Jeong, K. H. Kim, S. Lee, M. C. Choi, S. Q. Choi, *Langmuir* **2014**, *30*, 14369. c) S. Y. Lee, B. R. Lee, J. Lee, S. Kim, J. K. Kim, Y. H. Jeong, S. Jin, *Int. J. Mol. Sci.* **2013**, *14*, 20157. d) C. A. Day, M. Kang, *Membranes* **2023**, *13*, 492. e) Y. Gambin, R. Lopez-Esparza, M. Reffay, E. Sierecki, N. S. Gov, M. Genest, R. S. Hodges, W. Urbach, *Proc. Natl. Acad. Sci.* **2006**, *103*, 2098. f) M. Bennett, *Dependence of Cellular Behaviour on Viscosity Defined Ligand Mobility in Supported Lipid Bilayers [D]*, University of Glasgow, **2018**.

[22] K. Risse, J. L. Bridot, J. Yang, L. Sagis, S. Drusch, *J. Colloid Interface Sci.* **2025**, *686*, 203.

[23] F. Ruggeri, F. Zhang, T. Lind, E. D. Bruce, B. L. T. Lau, M. Cárdenas, *Soft Matter.* **2013**, *9*, 4219.

[24] X. Jia, K. Minami, K. Uto, A. C. Chang, J. P. Hill, T. Ueki, J. Nakanishi, K. Ariga, *Small* **2019**, *15*, 1804640.

[25] H. Peterlik, P. Roschger, K. Klaushofer, P. Fratzl, *Nat. Mater.* **2006**, *5*, 52.

[26] D. Kong, L. Peng, M. Bosch-Fortea, A. Chrysanthou, C. V. M. Alexis, C. Matellan, A. Zarbakhsh, G. Mastroianni, A. R. Hernandez, J. E. Gautrot, *Biomaterials* **2022**, *284*, 121494.

[27] K. J. Seu, A. P. Pandey, F. Haque, E. A. Proctor, A. E. Ribbe, J. S. Hovis, *Biophys. J.* **2007**, *92*, 2445.

[28] K. Ullmann, L. Poggemann, H. Nirschl, G. Leneweit, *Colloid Polym. Sci.* **2020**, *298*, 407.

